

Shuyue Ma · Haijun Qiu · Sheng Hu · Dongdong Yang · Zijing Liu

Characteristics and geomorphology change detection analysis of the Jiangdingya landslide on July 12, 2018, China

Abstract The reactivation of landslides has always been a prominent problem that has endangered town construction and people's safety worldwide. At about 8 a.m. on July 12, 2018, on a mountain near the Bailong River in Nanyu Township, Zhouqu County, Gansu Province, China, a landslide collapse event occurred. About 10,000 m³ of sloped material slid into the Bailong River, with the largest stone reaching 3 m³. As a result, a large number of houses were flooded. Highways and bridges were destroyed. Using field investigations, unmanned aerial vehicle (UAV) photography, InSAR traces, historical records, and multiple remote sensing images, we extracted the landslide's geometry and geomorphic parameters to quantify the characteristics of the Jiangdingya landslide. Based on high-resolution topographic data collected before and after the landslide, the change in the geomorphological factors, geomorphologic stability, and detection of the precursory motion before the landslide failure were analyzed to fully investigate the temporal geomorphological changes. Synthesizing the above research, we discuss the causes of landslide reactivation. The Jiangdingya landslide is a typical ancient landslide formed by the coupling of internal and external dynamics. Rainfall, seismic fault zone activity, human activities, and river erosion were the main causes of this reactivation event.

Keywords Ancient landslide · Reactivation · Geomorphological changes · UAVs · InSAR

Introduction

Zhouqu County, China, which is located in the North-South seismic belt, is affected by neotectonic movement with frequent earthquakes occurring since ancient times (Wang et al. 1994). Due to this seismic activity, geological disasters such as landslides, collapses, and debris flows have frequently occurred in Zhouqu County (Zhang and Huang 2018). In particular, the 2008 Wenchuan earthquake caused the collapse of many mountain slopes, the loosening of hillside deposits, and signs of reactivation in a large number of ancient landslides (Yang et al. 2014). The term "ancient landslides" generally refers to landslides that have slipped since the Quaternary, and they are the product of the long-term complex evolution of slopes (Zhang et al. 2018; Guo et al. 2019). Ancient landslide reactivation has seriously threatened the safety of the people's lives and property. For example, the Baitukan landslide in Kangding was partially reactivated in 1995, causing 33 deaths, injuring more than 100 people, and directly leading to the loss of 560 million Yuan (Yuan et al. 1998). The Cuifeng mountain landslide (Song 2014), the Beishan landslide (Xu 2015), the Shanmaoding #1 landslide (Fu 2017), and the landslide in Yanwotou, Luzhou, Sichuan (Zeng 2010) are all typical ancient landslide reactivation events, which destroyed buildings and roads, causing casualties and property losses.

At about 8 a.m. on July 12, 2018, a landslide event caused debris covering a 680 by 210 meter area, totaling 5,000,000 m³, to block a river in Jiangdingya, Nanyu Town, Zhouqu County (Fig. 1). Many roadbeds and bridges were washed away, a large number of houses in the villages of Nanyi and Naner were flooded, and more than 2300 people were evacuated. This landslide is a typical case of ancient landslide reactivation. There have been several devastating landslides in Jiangdingya throughout history (Chen 1991; Wang et al. 1994; Mu, 2011). In 1807, there was a large-scale landslide that blocked the river and slipped frequently afterward (Chen 1991; Guo et al. 2019). Since then, instances of sliding have occurred in 1985, 1986, 1988, 1990, and 1991 (Wang et al. 1994; Guo et al. 2019). On September 11, 1990, a landslide with a volume of millions of cubic meters pushed the Lianglang highway into the river. The soil accumulation rose as high as 5 to 15 m above the river. With the river partially blocked, the water level rose and some farmlands were inundated (Chen 1991). On the afternoon of June 13, 1991, more than six million m³ of landslide material destroyed the road and pushed it to the other side of the Bailong River. The toe that piled into the river was about 20-m high and about 250-m long. The river was blocked and its flow was interrupted for 9 h and 20 min, resulting in more than four million m³ of water being retained by the landslide. A total of 1403 rooms in Nanyu Township, 700-m upstream, were flooded, impacting 193 households and 869 people (Wang et al. 1994). Due to the strong measures taken by the Chinese government, there were no casualties as a result of this landslide. The landslide event that occurred on June 13, 1991, was a continuation of the September 11, 1990, landslide event.

In recent years, with the development of space-sky-ground observation technology, an increasing number of studies have revealed the characteristics of landslides, explored their sliding mechanisms, and monitored the movement of landslides (Wang 2013; Darren et al. 2015; Wartman et al. 2016; Guo et al. 2016; Cheng et al. 2018; Fan et al. 2018a; Cui et al. 2019; Hu et al. 2019; Martino et al. 2020; Catane et al. 2019; Guo et al. 2019; Yan et al. 2020; Zhou et al. 2020). For example, Zhuang and Peng (2014) selected the Bailu tableland landslide as a case study and investigated its triggering factors, formation process, and hazard characteristics using multiple methods, including 3D laser scanning, field investigations, and measurements. Catane et al. (2019) provided new insights into the initiation, transport, and deposition mechanisms of low-angle translational block slides using a combination of drone photogrammetry, video footage, satellite images, and field evidence. Ouyang et al. (2018) analyzed the failure mechanisms and characteristics of the 2016 catastrophic rockslide in Su Village, Lishui, China, using high-resolution remote sensing images and photos, video of the rockslide, and field investigations. Dai et al. (2019a) demonstrated the feasibility of

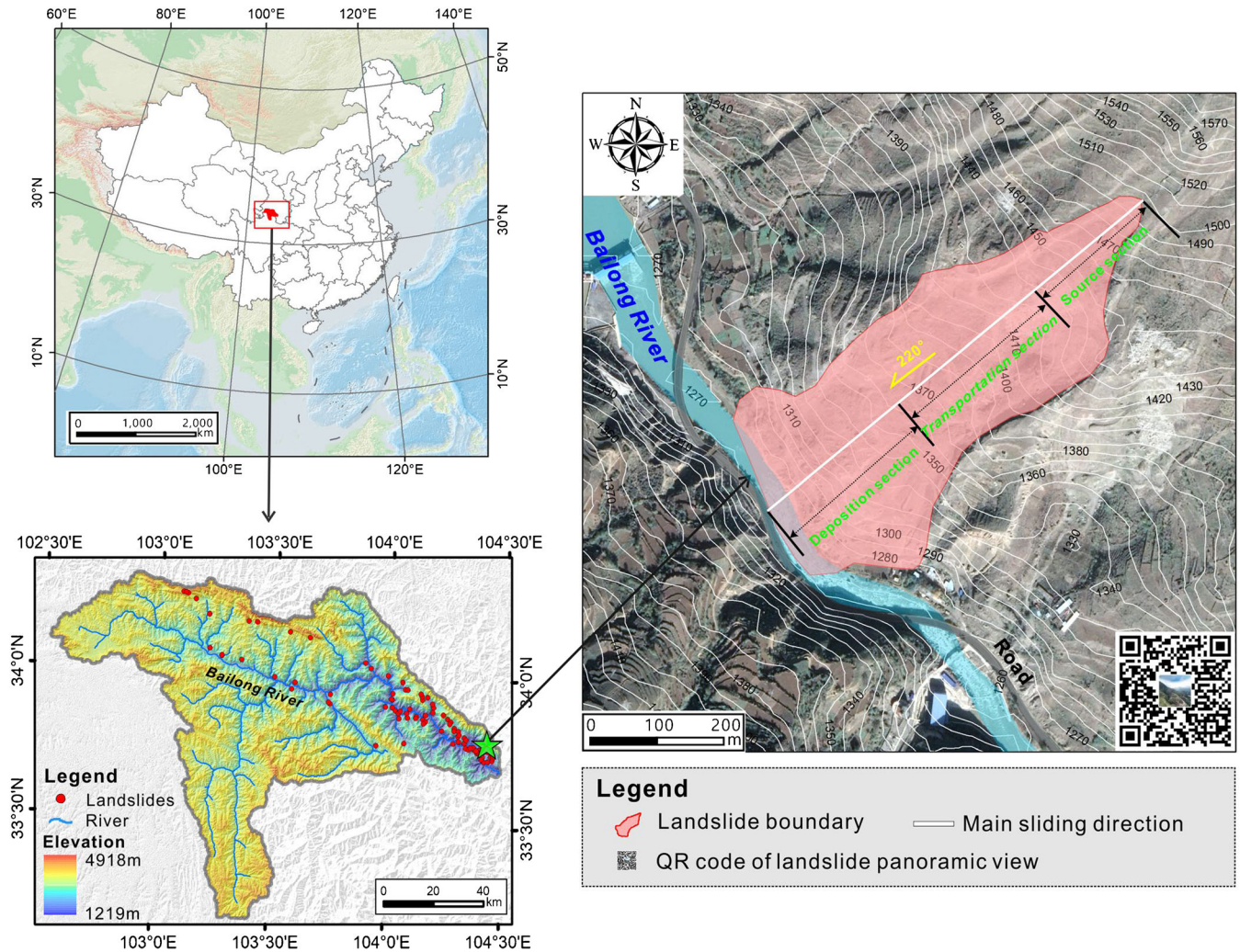


Fig. 1 The location and outline of the Jiangdingya landslide

performing timely and effective post-disaster assessment using spaceborne synthetic aperture radar (SAR) data, taking the 2017 catastrophic Xinmo landslide (Sichuan, China) as an example. However, in general, more attention has been paid to newly occurring landslides and less to the reactivation of old landslides. The high risk of ancient landslide reactivation deserves further research. Monitoring the reactivated behavior of ancient landslides is of great significance to the prevention of geological disasters.

Traditional field investigations and measurements of geological disasters are often time-consuming, laborious, and high-risk (Qiu et al. 2018). In recent years, non-contact measurement methods such as three-dimensional laser scanning, drone photogrammetry, and InSAR have been increasingly used for monitoring geological disasters. In particular, unmanned aerial vehicle (UAV) and InSAR technologies are highly complementary. UAVs are small in size and convenient in regard to portability and operation (Hu et al. 2019; Tian et al. 2020). Using UAVs in combination with aerial surveying and mapping systems can quickly obtain surface information, high-resolution images, and more accurate data. Most importantly, the data

collected by UAVs can be used to generate 2D and 3D visualization data such as digital elevation models (DEMs), digital orthophoto maps (DOMs), and 3D landscape models (Ouyang et al. 2018; Fan et al. 2018b; Ma et al. 2018). InSAR has advantages such as a high monitoring accuracy, wide spatial coverage, and short acquisition intervals, and it is only marginally affected by cloud cover (Zhang et al. 2016; Bayer et al. 2018; Dong et al. 2018; Lacroix et al. 2018; Dai et al. 2019a; Dai et al. 2019b; Teshebaeva et al. 2019). It is not only an effective supplement to traditional space remote sensing and photogrammetry methods, but it also exploits new observation methods and applications.

This paper uses the Jiangdingya landslide in Zhouqu, Gansu, China, as an example. By carrying out remote sensing image analysis, UAV surveys, InSAR deformation monitoring, and field surveys, the basic characteristics of the landslide are extracted, and the landform changes before and after the landslide occurred are analyzed. The deformation process before the landslide is investigated, and the submergence risk after the landslide is evaluated. Finally, the main factors influencing the reactivation of the ancient landslide are discussed and analyzed.

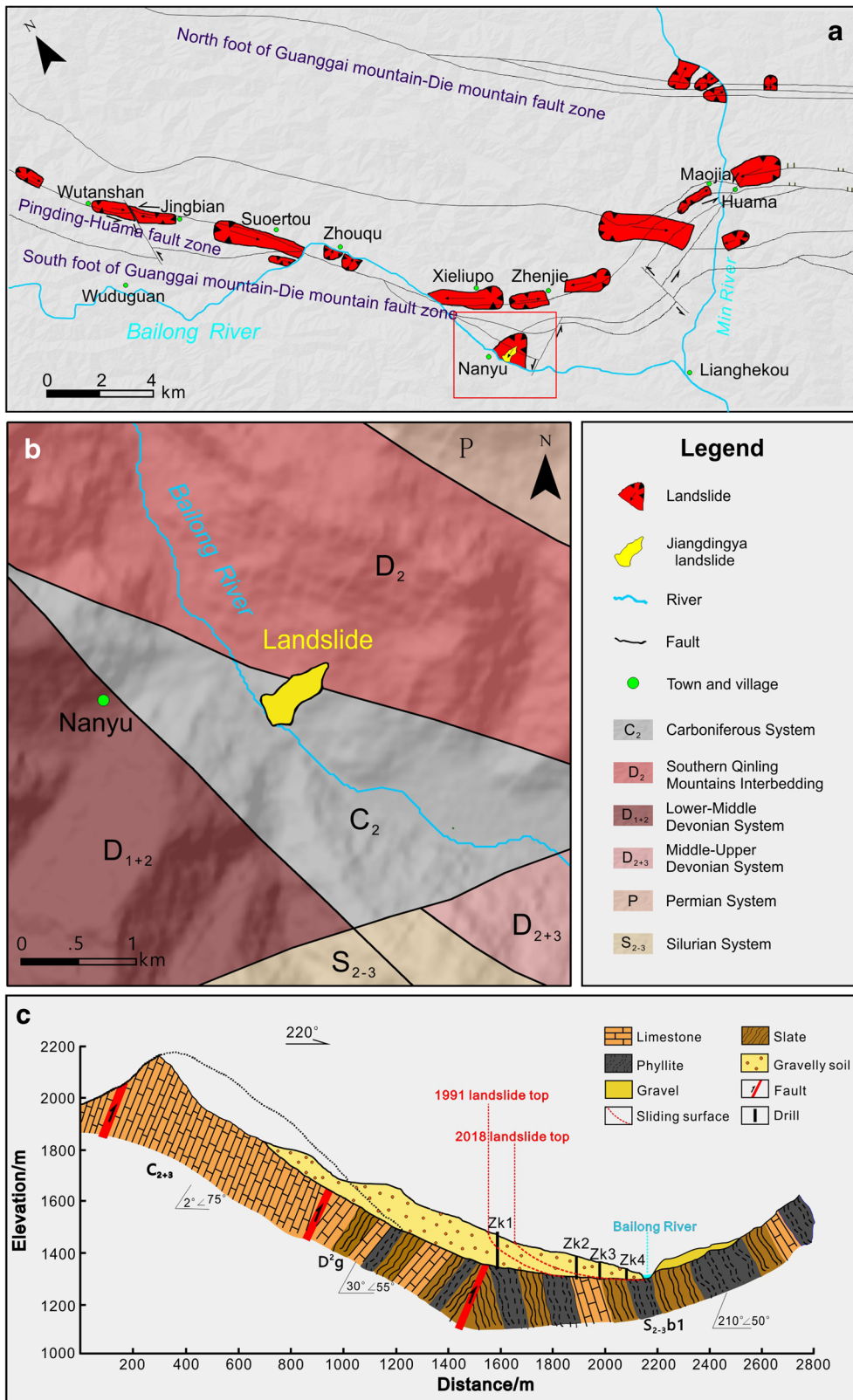


Fig. 2 The geologic environment around the Jiangdingya landslide. **a** The distribution of the faults and landslides around the Jiangdingya landslide adapted from Yang et al. (2014). **b** Geologic map of the Jiangdingya landslide. **c** Engineering geologic profile of the Jiangdingya ancient landslide adapted from Guo et al. (2019)

Recent Landslides

Table 1 Geometric characteristics of Jiangdingya landslide

Maximum elevation difference	Maximum length	Maximum width	Perimeter	Area
212.82 m	701 m	302.58 m	1815.58 m	147,193 m ²
Maximum stack thickness	Length/width ratio	Thickness/length ratio	Plane morphology	Profile morphology
26.80 m	2.32	0.04	Tongue shape	Concave

Data source

The images and terrain data collected before and after the landslide are from different data sources. We used pre-landslide DEMs from Google terrain data with a resolution of 8.7 m. The high-resolution post-landslide data were acquired via UAV (DJI Mavic Pro). The geological data are from the Geologic map of the Qinling Mountains-Daba Mountains (1:500,000) (Fig. 2b). The rainfall data are from the Zhouqu Meteorological Administration, which were collected at the Jiuzhai rainfall station. The data used in the time series SBAS-InSAR method are from the Sentinel-1 satellite. In this study, a total of 41 Sentinel-1 images were used, with a time span ranging from 2017-01-02 to 2018-07-08 and a time interval of 12 days. The data imaging mode is the interference wide mode, with a width of 250 km and a ground resolution of 5 m × 20 m. By setting

the time baseline threshold to 72 days and the vertical baseline threshold to 104 m, the data were mainly images taken on 2018-02-02, and all of the other images were accurately registered with the main image.

Geologic setting

The Jiangdingya landslide (33° 43' 32" N, 104° 25' 16.27" E) occurred in Zhouqu County, Gansu Province, on the left bank of the Bailong River (Fig. 1). The Bailong River is a perennial water system and is a first-class tributary of the Jialing River system in the Yangtze River Basin. There are high mountains and deep valleys around the landslide area, with steep and complex terrain. The study area has a temperate monsoon climate with a mean annual temperature of 14.1 °C. The precipitation in the area is affected by the East Asian

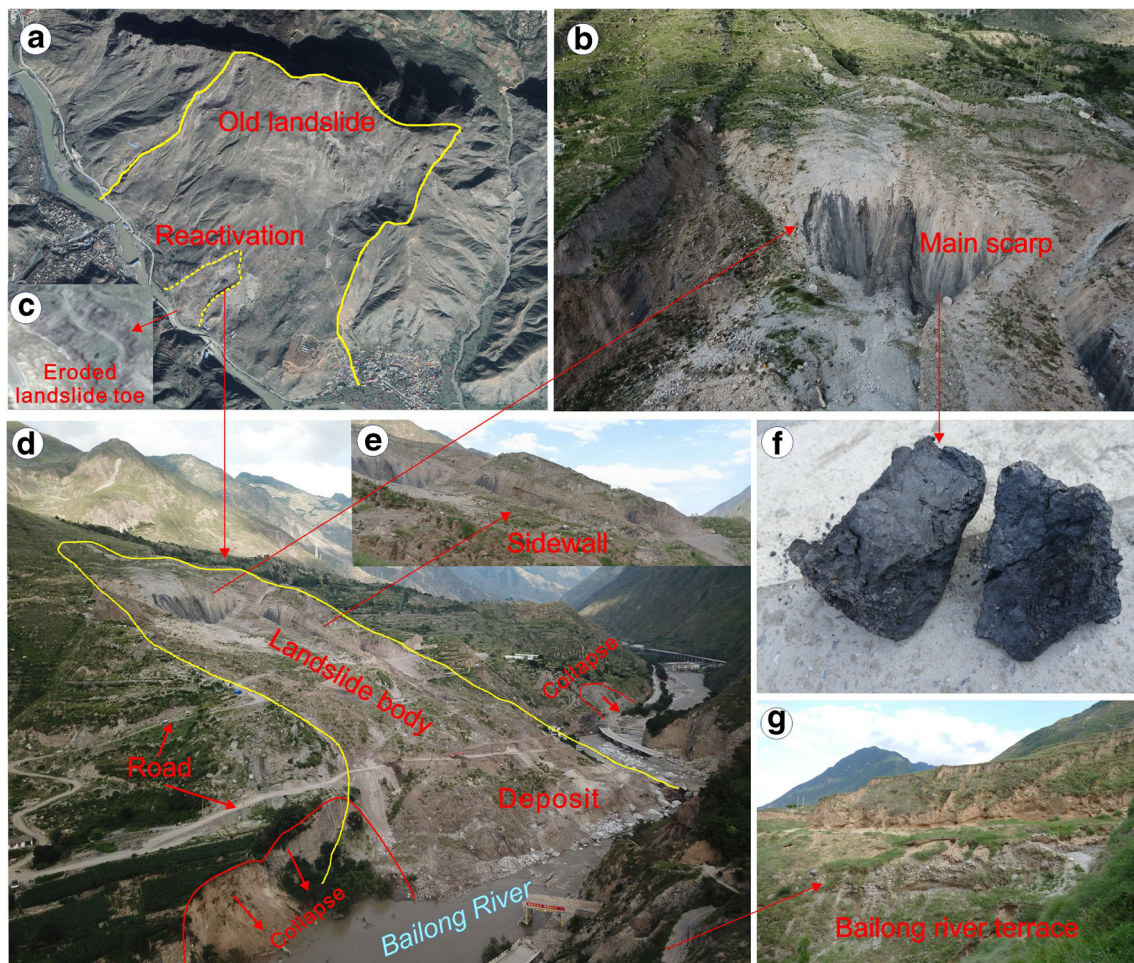


Fig. 3 Images of the July 12, 2018, Jiangdingya landslide

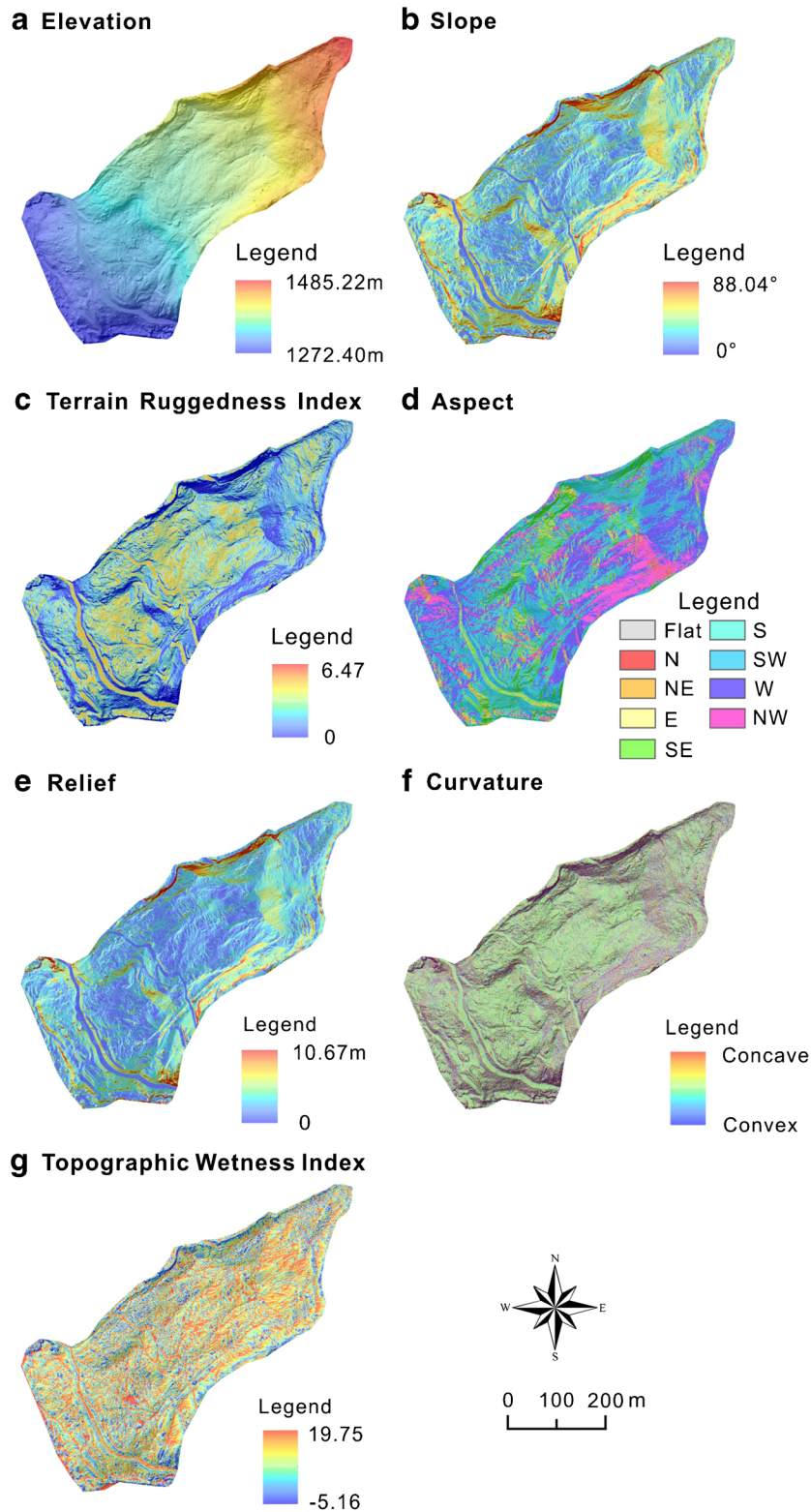


Fig. 4 Topographic characteristics of the Jiangdingya landslide

monsoon climate, and the intra-annual distribution is extremely uneven. The precipitation is mainly concentrated from May to October, accounting for 75.8% of the annual rainfall.

The complex topography and landforms and the development of fault structures make it a highly vulnerable area for geological disasters such as landslides and debris flows. The

Table 2 Topographic characteristics of Jiangdingya landslide

Index	Parameter	Statistic before landslide	Statistic after landslide
Elevation (m)	Max	1485.16	1485.16
	Mean	1358.25	1362.10
	Min	1277.16	1277.24
Slope (deg)	Max	26.58	52.05
	Mean	16.01	20.03
	Min	0.42	1.00
Aspect (deg)	Max	355.84	358.08
	Mean	223.16	228.67
	Min	10.23	2.33
Terrain ruggedness index	Max	2.95	9.82
	Mean	1.66	2.03
	Min	0.37	0.27
Relief (m)	Max	6.84	24.13
	Mean	3.36	5.63
	Min	0.00	0.00
Curvature	Max	7.08	34.68
	Mean	− 0.009	− 0.012
	Min	− 6.90	− 25.36
Topographic wetness index	Max	11.52	12.16
	Mean	5.97	5.04
	Min	2.71	1.97

lower portion of the Jiangdingya landslide is composed of Carboniferous strata, and the upper portion is composed of the Southern Qinling Mountains System (Fig. 2b). The landslide body is mainly composed of mixed pale-yellow limestone, carbonaceous slate, phyllite, and a small amount of loess (Fig. 2c). There is also a small amount of sandstone, breccia, gray-green schist, and shale fragments. Large limestone blocks can be found in the lower part of the landslide body. Due to the strong erosion by the Bailong River, the collapsed deposits have experienced multiple slips, making the slope's structure very mixed (Yang et al. 2013; Yang et al. 2014; Guo et al. 2019). The distribution and main sliding directions of nearby landslides are all controlled by fault zones and the regional tectonic activity, e.g., the Wutanshan landslide, the Jingbian landslide, the Suertou landslide, the Xieliupo landslide, the Zhenjie landslide, and the Maojia landslide (Fig. 2a). Furthermore, the study area is located in the North-South seismic belt. According to historical records, there have been multiple earthquakes with magnitudes of 6.0 or higher in this region (Yang et al. 2013; Yang et al. 2014; Zhang 2018). The reactivation frequency of landslides in this area is high, such as the Xieliupo landslide, the Nanyu landslide, and the Suertou landslide, which have been reactivated many times. At present, some of the landslides are still in continuous deformation and frequently cause new disasters.

Characteristics of the Jiangdingya landslide

Geometric characteristics

Using high-resolution terrain data, several geometric characteristic parameters were extracted using ArcGIS 10.5 and Global Mapper 17. High-resolution data, currently collected using UAVs, can show the spatial regularity of a landslide's interior in more detail than the lower resolution of conventional and free data (Hu et al. 2018; Hu et al. 2019). The geometric characteristics of the Jiangdingya landslide (Table 1) can be used to directly describe the landslide's morphology (Qiu et al. 2016; Qiu et al. 2017). The sliding part of the main body is elongated, exhibiting a tongue shape (Fig. 3). The longest part of the landslide is 700 m, and the widest part is 302.58 m. The average thickness of the sliding body is about 30 m. The relative height difference is 212.82 m. The main sliding direction is 220°, and the total landslide volume is about five million m³.

Topographic characteristics

Based on the high-resolution DEM data obtained using UAVs, the topographic characteristics were calculated using SAGA 6.0. Fig. 4 shows the spatial distribution maps of seven terrain factors: elevation, slope, aspect, terrain ruggedness index (TRI), relief, curvature, and topographic wetness index (TWI). In addition, Table 2 shows the maximum, mean, and minimum values of the elevation, slope, aspect, TRI, relief, curvature, and TWI, which can be used to

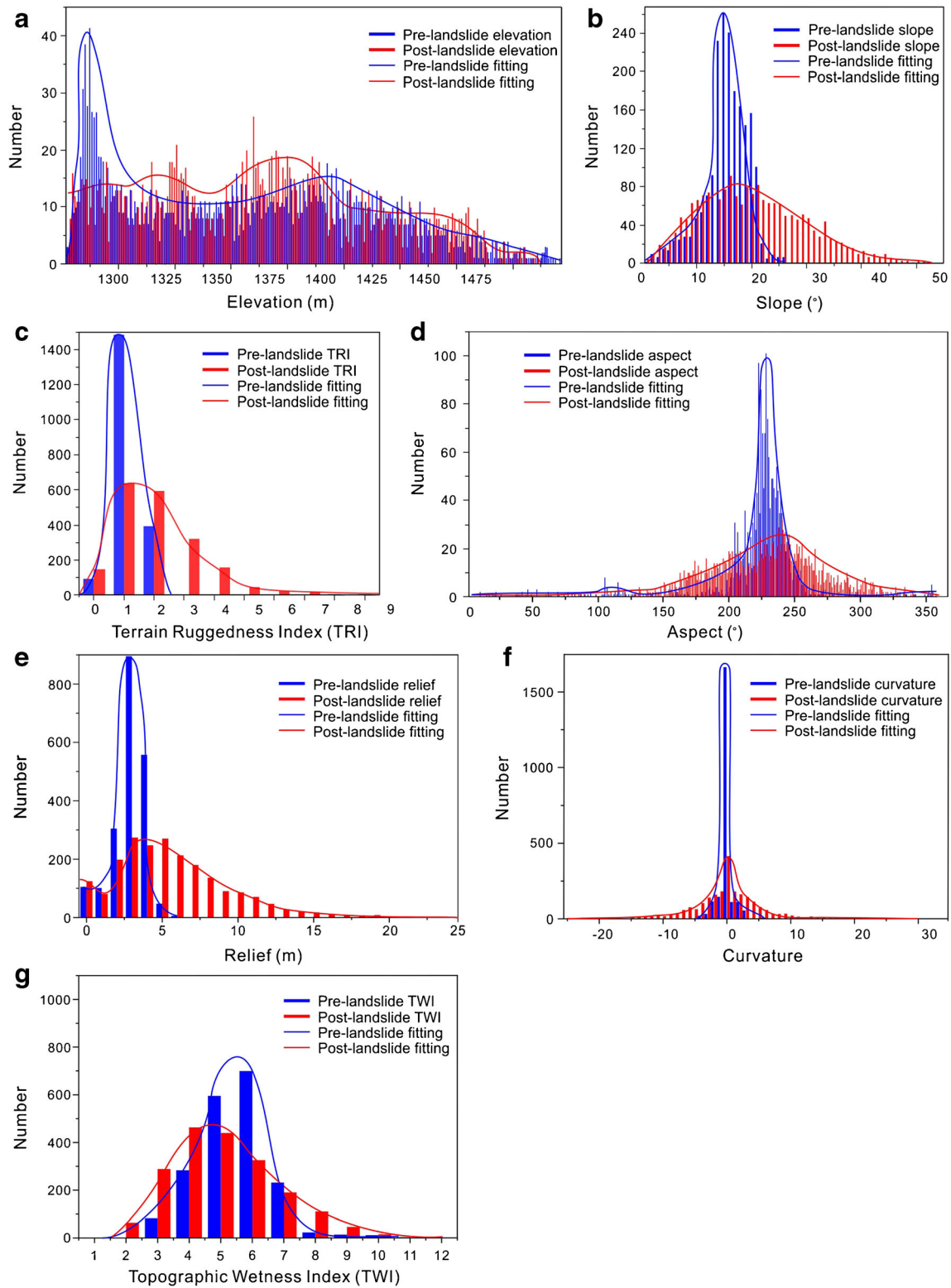


Fig. 5 Topographic characteristic change of the Jiangdingya landslide

express the landslide's topographic characteristics. The slope gradient is mainly 10° – 30° . The aspects of the landslide are mostly toward the southwest. The TRI of the deposition of landslide is

significant. The higher relief values are located on the main scarp. The areas with high TWI values are mainly distributed along the hydrological path on the landslide's body. These high value areas

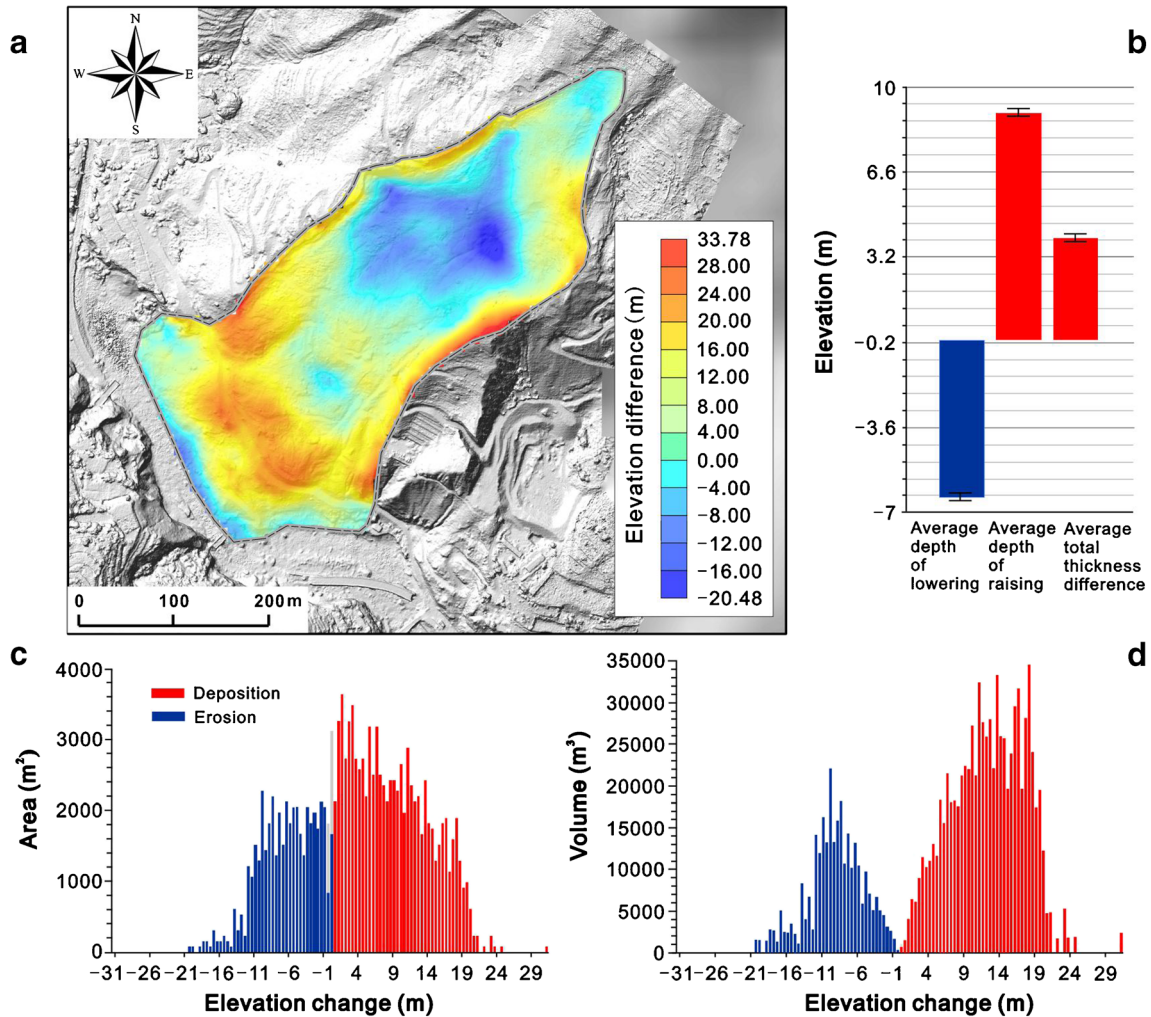


Fig. 6 Geomorphic change detection. **a** Elevation difference change before and after the landslide. **b** Average depths of lowering, raising, and thickness difference of the elevation difference. **c** elevation change distribution based on area. **d** elevation change distribution based on volume

will be more severely eroded by flowing water in the future and will also have a certain impact on the stability of the landslide.

Geomorphological changes

Geomorphological factor changes

By quantitatively comparing the seven terrain factors before and after the landslide occurred, we can clearly observe the geomorphological changes of the Jiangdingya landslide. By resampling the data from the different DEM data sources, the pre-landslide and post-landslide DEMs are at the same level of precision for the

comparison and analysis. Figure 5 shows the geomorphological changes before and after the landslide. Table 2 presents mean values change. As can be seen, the classification distribution of each factor after the landslide between is more uniform than before the landslide. This indicates that the landslide terrain changed drastically. The landslide had a strong shaping effect on the original landforms.

In order to better detect the dynamic processes of the landslide, we applied the widely used geomorphic change detection software (GCD) 7.0 to analyze the geomorphic changes between the two surveys (Wheaton 2014; Pasternack and Wyrick 2017; Shahverdian

Table 3 Statistics of geomorphological change in area and volume before and after landslide

	Area (m ²)	Volume (m ³)	Percent (by volume)	Average depth (m)
Surface lowering	43,673	285,058 ± 6176 (2%)	74%	6.53 ± 0.14 (2%)
Surface raising	90,979	811,682 ± 12,866 (2%)	26%	8.92 ± 0.14 (2%)
Total change	134,653	1,096,739 ± 19,043 (2%)	48% (net to total volume ratio)	8.00 ± 0.14 (2%)

Percent imbalance (departure from equilibrium) = 24%

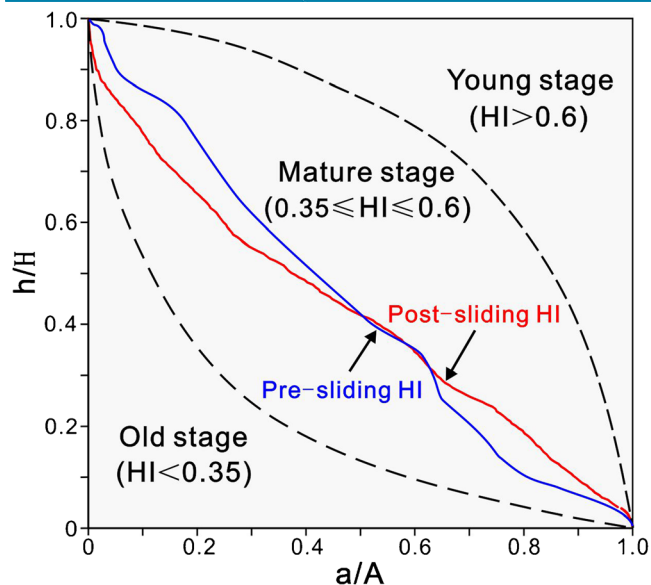


Fig. 7 Hypsometric integral change before and after the landslide

et al. 2017; Hu et al. 2019). Figure 6 and Table 3 present the statistics of the geomorphological changes in the area and volume before and after the landslide, which were quantified using GCD analysis. The average net depth difference is about 3.84 ± 0.10 m. The erosion volume is $285,058 \pm 6176$ m³, and the deposition volume is $811,682 \pm 12,866$ m³. The percent of the surface lowering volume is about 74%, and that of the surface raising volume is about 26%. The elevation changes due to erosion range from -20.48 to 0 m, while the elevation of the deposition ranges from 0 to 33.78 m. The net difference in the erosion and deposition volumes is $526,624 \pm 14,272$ m³.

Geomorphologic stability

Davis 1889 proposed the theory of geomorphic cycles and concluded that the process of landform development can be divided into three stages: young, mature, and old. Strahler (1952)

classified the development stages of geomorphology using the hypsometric integral (HI) values for basin geomorphology. Landslides are a form of slope landform. Thinking of them as a simple and small basin, we used the HI to analyze the geomorphologic stability and changes before and after the landslide (Hu et al. 2019). The integral curve uses the relative height ratio (h/H) in the basin as the vertical axis and the relative area ratio (a/A) as the horizontal axis. Where a is the cross-sectional area of a certain height in the basin, A is the total area of the basin, h is the height difference between a certain elevation and the lowest elevation in the basin, and H is the maximum height difference in the basin. The HI value is the area enclosed by the area elevation integral curve and the abscissa coordinate axis. The integral curve and the HI value can reflect the development stage of the basin's geomorphology, which correspond to the three stages of Davis's erosion cycle theory. When $HI > 0.6$, the geomorphological development stage is young; when $0.35 \leq HI \leq 0.6$, the geomorphological development stage is mature; and when $HI < 0.35$, the geomorphological development stage is old. Figure 7 shows that the Jiangdingya landslide was in the mature stage both before and after the landslide. The calculation results show little change in the HI values. Moreover, the integral curve not only reflects the overall stability, but it also reflects the interior morphology of the landslide (Hu et al. 2018). When the pre-sliding HI curve plots below the post-sliding HI curve, this indicates that erosion is occurring; however, when the pre-sliding HI curve plots above the post-sliding HI curve, this indicates that deposition is occurring.

Detection of precursory motions before landslide failures

InSAR technology utilizes synthetic aperture radar (SAR) images obtained from observations at the same orbit and in the same area to conduct interference differential processing (Marko et al. 2015; Sun et al. 2015; Tomás et al. 2016; Dai et al. 2016; Zhang et al. 2018; Dai et al. 2019a; Yang et al. 2019). After removing the residual errors of the topography, the atmospheric effects, and other relevant errors, the high-precision three-dimensional topography and information on the micro-ground deformation can be obtained (Handwerger et al. 2013; Singleton et al. 2014; Lacroix et al. 2018; Yang et al. 2019). InSAR has played an important role in monitoring the deformation of large landslides and in surveying landslides, providing strong support for the analysis of landslide-inducing factors and post-disaster stability assessment. Inspired by previous studies (Sun et al. 2015; Zhang et al. 2016; Dai et al. 2016; Dong et al. 2018; Dai et al. 2019a; Dai et al. 2019b), we used the time series SBAS-InSAR (small baseline subset InSAR) method, based on the two-dimensional deformation of the landslide obtained from Sentinel-1 radar images, to investigate the evolution of the slope before the landslide. The relationship between the spatial-temporal baseline and the dates of the ascending orbit data is shown in Fig. 8. The figure shows the distribution results of the deformation in the Jiangdingya landslide area (Fig. 9). From these results, it can be seen that the middle region of the landslide body exhibits the most severe deformation (Fig. 10a). In addition, there is another significantly deformed slope in the northern part of the landslide, which is a sign of a potential future landslide (Fig. 9). The maximum deformation rate reached 30 mm/a, and the maximum cumulative deformation value reached 47 mm. Furthermore, as can also be seen from the historical images (2010–2018),

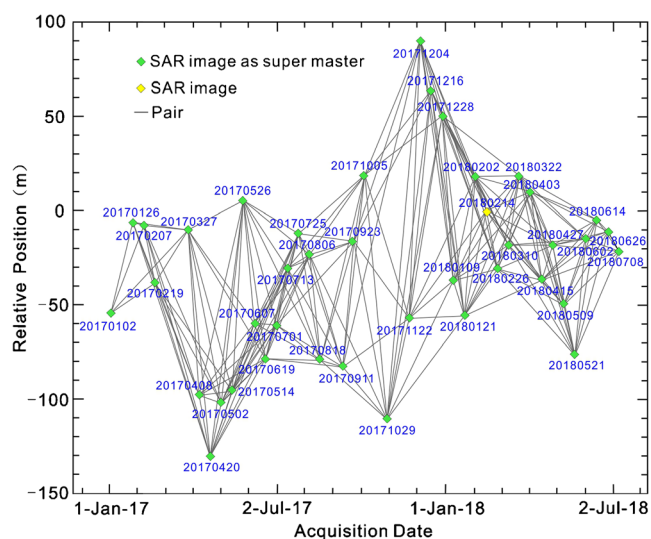


Fig. 8 The spatial and temporal baselines

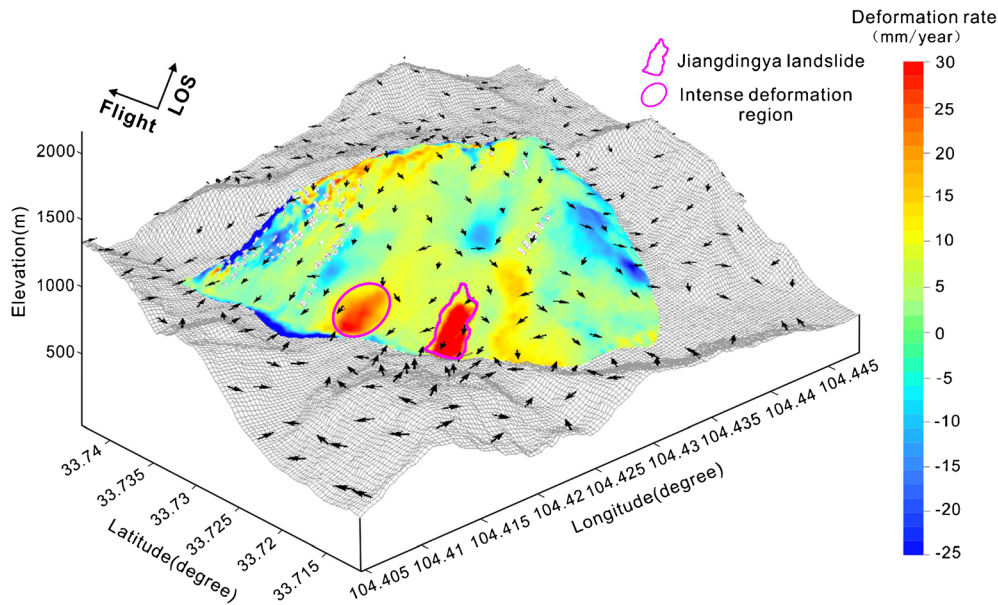


Fig. 9 The line of sight (LOS) deformation rate map from the Sentinel-1 data (black arrows indicate the directions of the maximum topographic gradient)

the landslide has been in a stage of creep, with the main scarp constantly retreating (Fig. 11). Six points were selected in the landslide deformation area and the adjacent area to display the cumulative deformation time series results, which reflect the deformation differences in the different areas. Combined with the rainfall data, the displacement time series show that there are two stages of deformation evolution and that there is a clear relationship between rainfall and deformation (Fig. 10b). In particular, from spring to summer (February to July), the rainfall and the deformation both increased significantly. Thus, rainfall is the main inducing factor of landslide reactivation.

Discussion of the causative factors of the Jiangdingya landslide

Rainfall

Sustained and concentrated rainfall played a significant role in inducing the failure of the landslide (Qiu et al. 2020). By analyzing the rainfall within 72 h before the landslide occurred, we found that the precipitation was concentrated at 30–39 h before the landslide. In particular, in the 37th hour, the rainfall reached 23.4 mm. An interesting phenomenon is that no rain occurred about 24 h before the landslide, and a large amount of precipitation occurred in the 48 to 24 h before the landslide (Fig. 12). This indicates that when the amount of rainfall is insufficient to make the landslide body lose stability, the deformation of the landslide body lags behind the rainfall. Landslides occur when the landslide body is broken and the structure is loose. Infiltrating rain increases the water content of the landslide. When the water seeps into the impervious layer of the landslide, the sliding zone becomes saturated, and the shear strength of the sliding body is reduced. As the rainfall continues, the landslide body becomes more saturated and the groundwater level increases. The hydrodynamic pressure and the hydrostatic pressure of the landslide body increase and the weight of the rock and soil increases. After a period of rainfall, the landslide deformation continues until the

sliding force of the sliding body is greater than the friction force, at which time the landslide occurs.

Tectonic movement

Tectonic movement is the basis and geological factor of the landslide. Due to the influence of fault activity, fault zone landslides have re-occurred many times throughout history. Fault zone landslides are generally large-giant ancient landslides. The main scarp is the ridge and the toe is the river or secondary gullies. The Nanyu landslide is cut by three major faults (Yang et al. 2014; Guo et al. 2019; Guo et al. 2020). They divide the stratum and control and influence the direction of mountains so that the mountain appears as a developed fault block, forming a typical structural failure zone with strong damage. The landslide is located in the subsidence block between the three faults and in the structural failure zone. Its stability is extremely poor under the influence of tectonic movement.

River erosion

From the basic conditions and triggering factors of landslide formation, the three conditions of slope structure, stratigraphic lithology, and effective free face are indispensable. In the historical remote sensing images and field investigation, we found the trace of river erosion (Fig. 3c, d). Figure 3c shows the eroded landslide toe and Fig. 3d displays other small collapses on the concave bank of river. The toe of the slope is constantly eroded and eventually collapsed. River erosion can cause vacant surfaces on both sides of the valley. With the passage of time, the river continues to scour, with the valley experiencing down-cutting erosion and side erosion on the concave bank of the river. When the free surface cannot support the landslide body, the gravitational force on the landslide body causes it to lose stability and the slope slides into the river. The barrage lakes formed cause the water levels in upstream areas to rise. The Bailong River has a large and fast flow rate, especially during the rainy season, resulting in the transport of sediment and

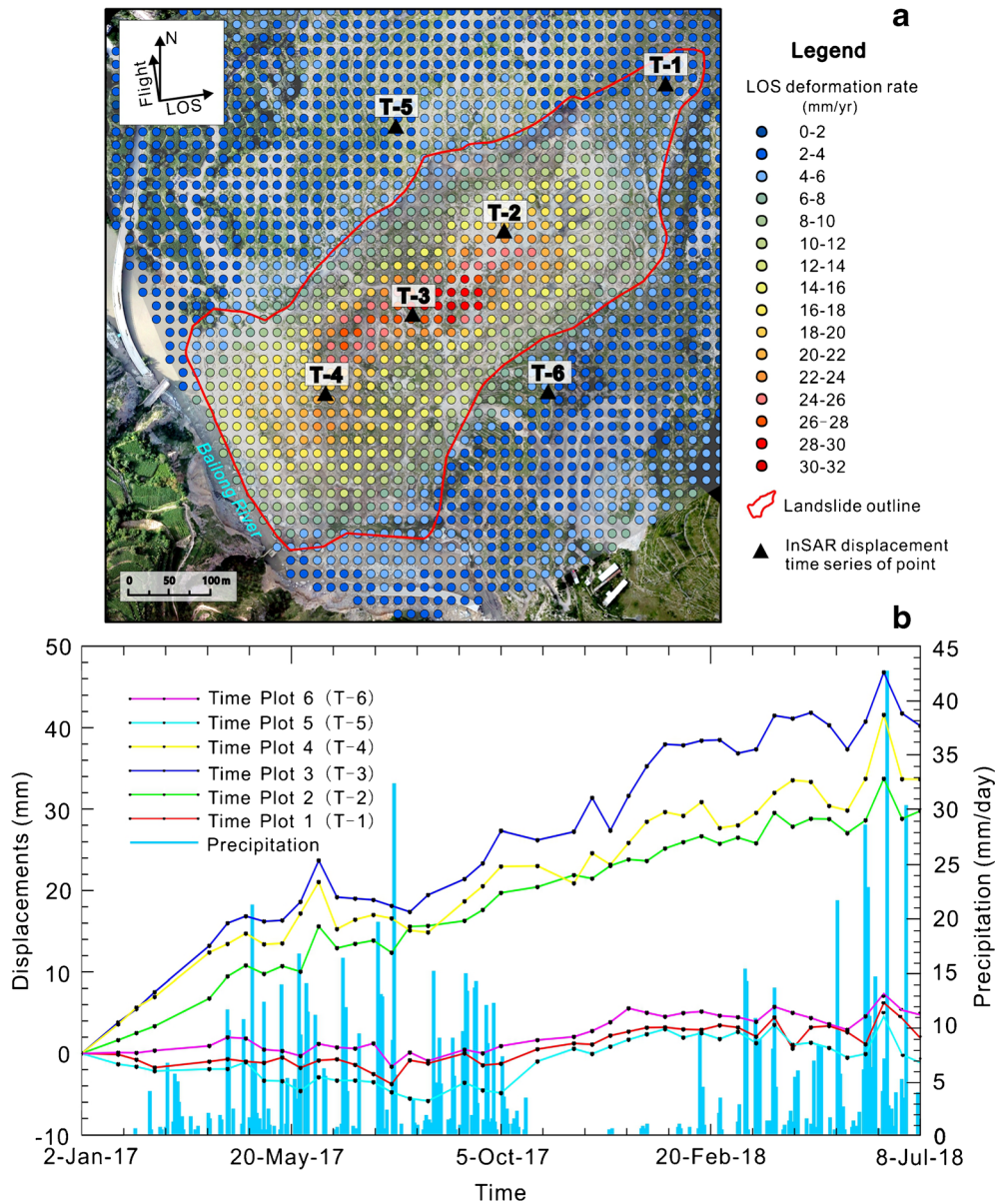


Fig. 10 a The LOS deformation rate map of the landslide. (b) InSAR displacement time series of six points

erosion. The river erodes the toe of the landslide, causing the landslide's stability to decrease.

Human activities

Human activities also disturbed the rock and soil mass of the landslide body and affected the stability of the ancient landslide (Zhang et al. 2013). There are increasing traces of human activities shown in Fig. 11. Part of the landslide has been transformed into farmland by local villagers, resulting in relatively wet conditions. There are trails and road on the landslide, which break the soil structure and reduce the landslide's stability. In particular, the S313 provincial highway passes through the toe area of the ancient landslide. In addition to daily human activities, human engineering activities have significantly decreased the

stability of the landslide, such as the excavation and movement of soil and rock.

Conclusions

The Jiangdingya landslide occurred on July 12, 2018. It is a typical reactivated landslide triggered by heavy precipitation. This study used multiple approaches from multiple perspectives to explore the changes before and after landslide and to determine their causes based on filed investigations, low-cost UAVs, and InSAR. The distribution of the geomorphological factors became gentle after the landslide. The stability of the geomorphology is still in the mature stage. Based on these results and the analysis of the rainfall data, we found that the deformation process before the landslide can be divided into accumulation and accelerating deformation stages,

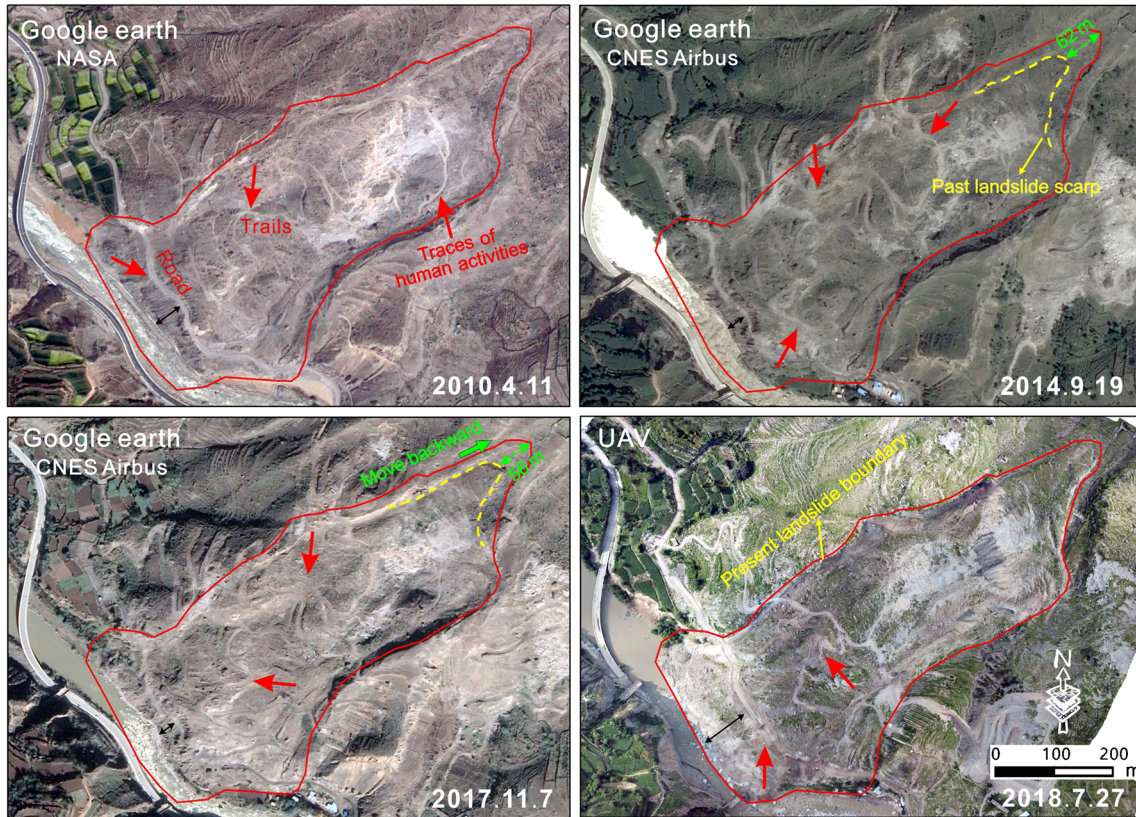


Fig. 11 Multi-images contrast of the Jiangdingya landslide (2010–2018). The red arrows represent traces of human activities

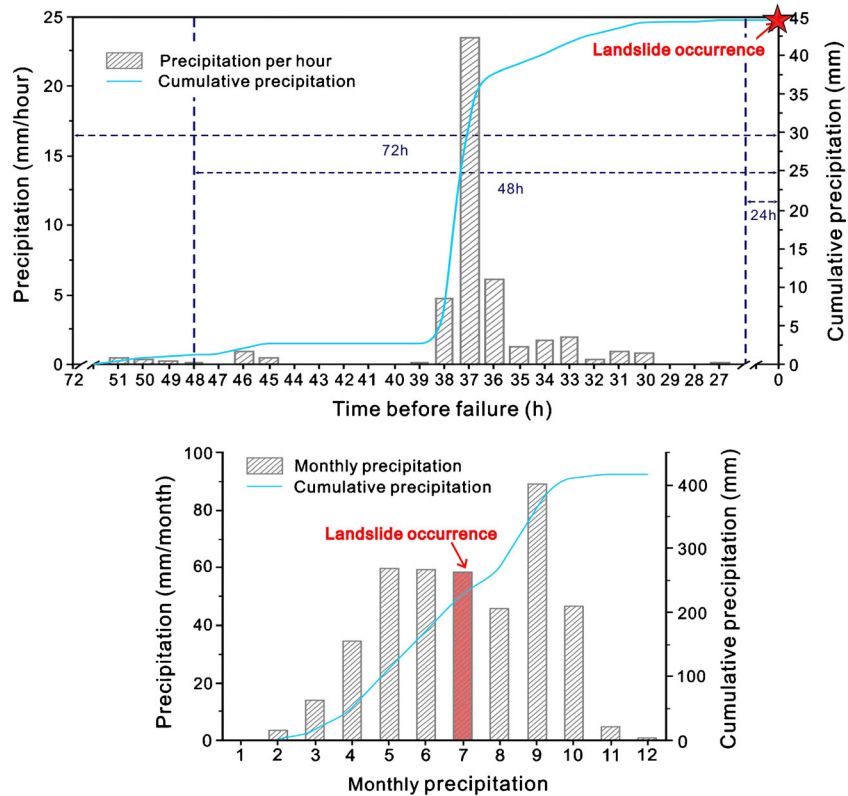


Fig. 12 Hourly precipitation before the landslide and the annual monthly precipitation

which are consistent with the rainfall. The reactivation of ancient landslides is caused by the coupling of internal and external dynamics, with the main causes including rainfall, seismic fault zone activity, river erosion, and human activities. Rainfall is the primary inducing factor. Through field investigations and analysis, we conclude that the potential energy of the landslide has not been fully released. Due to the impacts of external adverse factors such as erosion by the Bailong River, rainstorms, and earthquakes, reactivation may occur. It is recommended that comprehensive management of the Jiangdingya landslide area be implemented, such as anti-slide pile engineering, scaling engineering, interception and drainage engineering, and vegetation restoration engineering.

Funding

This work was funded by the Second Tibetan Plateau Scientific Expedition and Research Program (STEP) (Grant No. 2019QZKK0902), International Science & Technology Cooperation Program of China (Grant No. 2018YFE0100100), National Natural Science Foundation of China (Grant No. 41771539), Strategic Priority Research Program of Chinese Academy of Sciences (Grant No. XDA20030301), International Partnership Program of Chinese Academy of Sciences (Grant No. 131551KYSB20160002), China Postdoctoral Science Foundation (Grant No. 2019 M663792), and Scientific Research Foundation of Northwest University (Grant No. 360051900075).

References

Bayer B, Simoni A, Mulas M, Corsini A, Schmidt D (2018) Deformation responses of slow moving landslides to seasonal rainfall in the Northern Apennines, measured by InSAR. *Geomorphology* 308(1):293–306

Catane SG, Veracruz NAS, Flora JRR, Go CMM, Santos ERU (2019) Mechanism of a low-angle translational block slide: evidence from the September 2018 Naga landslide, Philippines. *Landslides* 16:1709–1719

Chen H (1991) Brief Introduction of Nanyu Large Landslide in Zhouqu County, Gansu. *Northwest Hydropower* 4:63

Cheng D, Cui Y, Su F, Jia Y, Choi CE (2018) The characteristics of the Mocoa compound disaster event, Colombia. *Landslides* 15:1223–1232

Cui Y, Cheng D, Choi CE, Jin W, Lei Y, Kargel JS (2019) The cost of rapid and haphazard urbanization: lessons learned from the Freetown landslide disaster. *Landslides* 16:1167–1176

Dai K, Li Z, Tomás R, Liu G, Yu B, Wang X, Cheng H, Chen J, Stockamp J (2016) Monitoring activity at the Daguangbao mega-landslide (China) using Sentinel-1 TOPS time series interferometry. *Remote Sens Environ* 186:501–513

Dai K, Xu Q, Li Z, Tomás R, Fan X, Dong X, Li W, Zhou Z, Gou J, Ran P (2019a) Post-disaster assessment of 2017 catastrophic Xinmo landslide (China) by spaceborne SAR interferometry. *Landslides* 16:1189–1199

Dai K, Zhuo G, Xu Q, Li Z, Li W, Guan W (2019b) Tracing the pre-failure two-dimensional surface displacements of Nanyu landslide, Gansu Province with Radar Interferometry. *Geomatics Inform Sci Wuhan Univ* 44(12):1778–1786

Darren T, Arko L, Steven DJ (2015) Time series analysis of landslide dynamics using an unmanned aerial vehicle (UAV). *Remote Sens* 7(2):1736–1757

Davis WM (1889) The rivers and valleys of Pennsylvania. *Natl Geogra Soc*

Dong J, Liao M, Xu Q, Zhang L, Tang M, Gong J (2018) Detection and displacement characterization of landslides using multi-temporal satellite SAR interferometry: A case study of Danba County in the Dadu River Basin. *Eng Geol* 240:95–109

Fan X, Xu Q, Scaringi G, Zheng G, Huang R, Dai L, Ju Y (2018a) The “long” runout rock avalanche in Pusa, China, on August 28, 2017: a preliminary report. *Landslides* 16:139–154

Fan X, Zhan W, Dong X, Van Westen CJ, Xu Q, Dai L, Yang Q, Huang R, Havenith HB (2018b) Analyzing successive landslide dam formation by different triggering mechanisms: the case of the Tangjiawan landslide, Sichuan, China. *Eng Geol* 243:128–144

Fu X (2017) Research on revival mechanism and stability of disturbed ancient landslide. Xihua University, Chengdu

Guo C, Zhang Y, Montgomery DR, Du Y, Zhang G, Wang S (2016) How unusual is the long-runout of the earthquake-triggered giant Luanshibao landslide, Tibetan Plateau, China? *Geomorphology* 259(15):145–154

Guo C, Ren S, Li X, Zhang Y, Yang Z, Wu R, Jin J (2019) Development characteristics and reactivation mechanism of the Jiangdingya ancient landslide in the Nanyu Town, Zhouqu County, Gansu Province. *Geoscience* 33(1):206–217

Guo C, Zhang Y, Li X, Ren S, Yang Z, Wu R, Jin J (2020) Reactivation of giant Jiangdingya ancient landslide in Zhouqu County, Gansu Province, China. *Landslides* 17:179–190

Handwerker AL, Roering JJ, Schmidt DA (2013) Controls on the seasonal deformation of slow-moving landslides. *Earth Planet Sci Lett* 377–378:239–247

Hu S, Qiu H, Wang X, Gao Y, Wang N, Wu J, Yang D, Cao M (2018) Acquiring high-resolution topography and performing spatial analysis of loess landslides by using low-cost UAVs. *Landslides* 15:593–612

Hu S, Qiu H, Pei Y, Cui Y, Xie W, Wang X, Yang D, Tu X, Zou Q, Cao P, Cao M (2019) Digital terrain analysis of a landslide on the loess tableland using high-resolution topography data. *Landslides* 16:617–632

Lacroix P, Bièvre G, Pathier E, Kniess U, Jongmans D (2018) Use of Sentinel-2 images for the detection of precursory motions before landslide failures. *Remote Sens Environ* 215:507–516

Ma S, Xu C, Shao X, Zhang P, Liang X, Tian Y (2018) Geometric and kinematic features of a landslide in Mabian Sichuan, China, derived from UAV photography. *Landslides* 16:373–381

Marko K, Holley R, Mahapatra P, Marel HVD, Bavec M (2015) Coupling of GPS/GNSS and radar interferometric data for a 3D surface displacement monitoring of landslides. *Landslides* 12:241–257

Martino S, Antonielli B, Bozzano F, Caprari P, Discenza ME, Esposito C, Fiorucci M, Iannucci R, Marmoni GM, Schilirò L (2020) Landslides triggered after the 16 August 2018 Mw 5.1 Molise earthquake (Italy) by a combination of intense rainfalls and seismic shaking. *Landslides* 17:1177–1190

Mu P (2011) Analysis on causes and stability of landslide at Jiangdingya in Zhouqu County of Gansu. *China Water Resour* 4:50–52

Ouyang C, Zhao W, Xu Q, Peng D, Li W, Wang D, Zhou S, Hou S (2018) Failure mechanisms and characteristics of the 2016 catastrophic rockslide at Su village, Lishui, China. *Landslides* 15:1391–1400

Pasternack GB, Wyrick JR (2017) Flood-driven topographic changes in a gravel-cobble river over segment, reach, and morphological unit scales. *Earth Surf Process Landf* 42(3):487–502

Qiu H, Cui P, Hu S, Liu Q, Wang Y, Gao Y (2016) Size-frequency distribution of landslides in different landforms on the Loess Plateau of Northern Shaanxi. *Earth Sci* 41(2):343–350

Qiu H, Cui P, Regmi AD, Hu S, Wang X, Zhang Y, He Y (2017) Influence of topography and volume on mobility of loess slides within different slip surfaces. *Catena* 157:180–188

Qiu H, Cui P, Regmi A, Hu S, Wang X, Zhang Y (2018) The effects of slope length and slope gradient on the size distributions of loess slides: Field observations and simulations. *Geomorphology* 300:69–76

Qiu H, Cui Y, Pei Y, Yang D, Hu S, Wang X, Ma S (2020) Temporal patterns of nonseismically triggered landslides in Shaanxi Province, China. *Catena* 187:104356

Shahverdian S, Macfarlane W, Stevens G, Meier M, Wheaton JM (2017) Geomorphic response to Pilot River Restoration on the San Rafael River. A Pilot Installation of Beaver Dam Analogues, Utah Retrieved from <https://doi.org/10.13140/RG.2.2.18963.37928>

Singleton A, Li Z, Hoey T, Muller JP (2014) Evaluating sub-pixel offset techniques as an alternative to D-InSAR for monitoring episodic landslide movements in vegetated terrain. *Remote Sens Environ* 147:133–144

Song S (2014) Formation mechanism analysis of Cuifengshan landslide in Lingshi County. *Shanxi Architecture* 40(36):74–75

Strahler AN (1952) Hypsometric (area-altitude) analysis of erosional topography. *Geol Soc Am Bull* 63(11):1117–1142

Sun Q, Zhang L, Ding X, Hu J, Li Z, Zhu J (2015) Slope deformation prior to Zhouqu, China landslide from InSAR time series analysis. *Remote Sens Environ* 156:45–57

Teshebaeva K, Ehtler HP, Bookhagen B, Strecker MR (2019) Deep-seated gravitational slope deformation (DSGSD) and slow moving landslides in the southern Tien Shan Mountains: new insights from InSAR, tectonic, and geomorphic analysis. *Earth Surf Process Landf* 44:2333–2348. <https://doi.org/10.1002/esp.4648>

Tian S, Chen N, Wu H, Yang C, Zhong Z, Rahman MM (2020) New insights into the occurrence of the Baige landslide along the Jinsha River in Tibet. *Landslides* 17:1207–1216

- Tomás R, Li Z, Lopez-Sanchez JM, Liu P, Singleton A (2016) Using wavelet tools to analyse seasonal variations from InSAR time-series data: a case study of the Huangtupo landslide. *Landslides* 13:437–450
- Wang G (2013) Lessons learned from protective measures associated with the 2010 Zhouqu debris flow disaster in China. *Nat Hazards* 69(3):1835–1847
- Wang J, Qi L, Cui X (1994) Analysis on landslide of Nanyu in Zhouqu county of Gansu province. *Bull Soil Water Conserv* 14(1):57–60
- Wartman J, Montgomery DR, Anderson SA, Keaton JR, Benoit J, Chapelle J, Gilbert R (2016) The 22 March 2014 Oso landslide, Washington, USA. *Geomorphology* 253(15):275–288
- Wheaton JM (2014) Trends and challenges in geomorphic change detection. Retrieved from <https://doi.org/10.13140/RG.2.2.26758.68167>
- Xu J (2015) Discussion on causes and prevention and control measure of landslide geological disasters in Yuci Beishan. *Shanxi Archit* 41(24):85–86
- Yan Y, Cui Y, Tian X, Hu S, Liao L (2020) Seismic signal recognition and interpretation of the 2019 “7.23” Shuicheng landslide by seismogram stations. *Landslides* 17:1191–1206
- Yang W, Huang X, Zhang C, Liu T (2013) The deformation characteristics of the landslide along Pingding-Huama active fault zone and its prevention and control. *Geol Bull China* 32(12):1925–1935
- Yang W, Huang X, Zhang C, Si H (2014) Deformation behavior of landslides and their formation mechanism along Pingding-Huama active fault in Bailongjiang River region. *J Jilin Univ (Earth Sci Ed)* 44(2):574–583
- Yang W, Wang Y, Sun S, Wang Y, Ma C (2019) Using Sentinel-2 time series to detect slope movement before the Jinsha River landslide. *Landslides* 16:1313–1324
- Yuan Y, Zheng W, Zheng Y, Zhu S (1998) The characteristics of the Baitukan Landslide in Kangdin, Sichuan and its countermeasures. *Chin J Geol Hazard Control* 9(S1):235–241
- Zeng Y (2010) Research on the mechanism of groundwater in reactivating of old landslides on Reservoir Bank. China University of Geosciences Wuhan China
- Zhang N (2018) Study on formation mechanism and comprehensive prevention of debris flow disasters in Sanyanyu valley, Zhouqu China. University of Geosciences Wuhan China
- Zhang F, Huang X (2018) Trend and spatiotemporal distribution of fatal landslides triggered by non-seismic effects in China. *Landslide* 15(8):1663–1674
- Zhang F, Wang G, Kamai T, Chen W, Zhang D, Yang J (2013) Undrained shear behavior of loess saturated with different concentrations of sodium chloride solution. *Eng Geol* 155(6):69–79
- Zhang Y, Meng X, Chen G, Qiao L, Zeng R, Chang J (2016) Detection of geohazards in the Bailong River Basin using synthetic aperture radar interferometry. *Landslides* 13:1273–1284
- Zhang Y, Wu R, Guo C, Wang L, Yao X, Yang Z (2018) Research progress and prospect on reactivation of ancient landslides. *Adv Earth Sci* 33(7):728–740
- Zhou S, Ouyang C, An H, Jiang T, Xu Q (2020) Comprehensive study of the Beijing Daanshan rockslide based on real-time videos, field investigations, and numerical modeling. *Landslides* 17:1–15
- Zhuang J, Peng J (2014) A coupled slope cutting—a prolonged rainfall-induced loess landslide: a 17 October 2011 case study. *Bull Eng Geol Environ* 73:997–1011

S. Ma · H. Qiu · S. Hu · D. Yang · Z. Liu

College of Urban and Environmental Sciences,
Northwest University,
Xi'an, 710127, China

S. Ma · H. Qiu · S. Hu · D. Yang · Z. Liu

Institute of Earth Surface System and Hazards,
Northwest University,
Xi'an, 710127, China

H. Qiu (✉) · S. Hu

Shaanxi Key Laboratory of Earth Surface System and Environmental Carrying Capacity,
Northwest University,
Xi'an, 710127, China
Email: haijunqiu@nwu.edu.cn